



Nokhbeh, S. R., Gholizadeh, M., Salimi, A., & Sparkes, H. A. (2020). Synthesis, crystal structure, Hirshfeld surface analysis, DFT calculations and characterization of 1,3-propanediylbis(triphenylphosphonium) monotribromide as brominating agent of double bonds and phenolic rings. *Journal of Molecular Structure*, 1206, Article 127700.
<https://doi.org/10.1016/j.molstruc.2020.127700>

Peer reviewed version

License (if available):
CC BY-NC-ND

Link to published version (if available):
[10.1016/j.molstruc.2020.127700](https://doi.org/10.1016/j.molstruc.2020.127700)

[Link to publication record on the Bristol Research Portal](#)
PDF-document

This is the author accepted manuscript (AAM). The final published version (version of record) is available online via Elsevier at <https://www.sciencedirect.com/science/article/pii/S0022286020300235>. Please refer to any applicable terms of use of the publisher.

University of Bristol – Bristol Research Portal

General rights

This document is made available in accordance with publisher policies. Please cite only the published version using the reference above. Full terms of use are available:
<http://www.bristol.ac.uk/red/research-policy/pure/user-guides/brp-terms/>

Synthesis, crystal structure, Hirshfeld surface analysis, DFT calculations and characterization of 1,3-propanediylbis(triphenylphosphonium) monotribromide as brominating agent of double bonds and phenolic rings

Seyed Reza Nokhbeh[†], Mostafa Gholizadeh^{†,*}, Alireza Salimi[†], Hazel A. Sparkes[‡]

[†]Department of Chemistry, Faculty of Science, Ferdowsi University of Mashhad, Mashhad, I.R., Iran

[‡]School of Chemistry, University of Bristol, Cantock's Close, Bristol BS8 1TS, UK

Keywords: phosphonium tribromide, Hirshfeld surface analysis, 2D fingerprint plots, Density Function Theory calculations, X-ray crystallography, brominating agent,

Supporting Information

Abstract: This paper presents synthesis and structural characterization of new members of phosphorus-based organic bromides. 1,3-Propanediylbis(triphenylphosphonium) dibromide **I** and 1,3-propanediylbis(triphenylphosphonium) monotribromide **II**, as a new brominating agent for double bonds and phenolic rings, were synthesized. ¹H NMR, ¹³C NMR, ³¹P NMR, FT-IR, single crystal X-ray diffraction crystallography, differential scanning calorimetry, thermogravimetric analysis and differential thermal analysis were used to characterize these salts. Thermal and physicochemical stability, simple working up, non-toxicity in comparison to liquid bromine and high yield are some of the advantages of these salts. These salts have good solubility in organic solvents, such as methanol, ethanol, acetone, dichloromethane and THF. Crystallographic data showed that compound **I** crystallized in the monoclinic crystal system, in *P*2₁ space group and compound **II** crystallized in the monoclinic crystal system, in *P*2₁/*c* space group and one of the bromide ions was replaced by tribromide ion in **II**. The crystal packing structures of title compounds were stabilized by various intermolecular interactions, especially of the type C-H... π contacts. The molecular Hirshfeld surface analysis and 2D fingerprint analysis revealed that the C...H (30.4 % for the compound **I** and 28.3 % for compound **II**) contact, which was related to C-H... π interactions, had the major contribution in the crystal architectures. To get more insight about molecular structures of titled compounds, DFT calculations were performed (energy, structural optimization and natural bond orbital analysis). Bromination of double bonds and phenolic rings was carried out to prove the ability of the tribromide salt to bromine such organic substrates.

Introduction

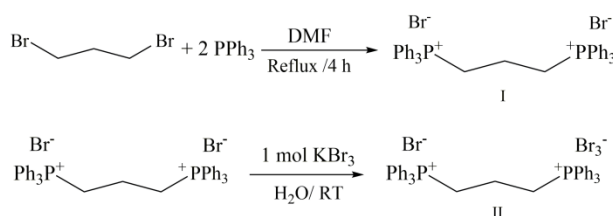
In recent years heteronium salts, especially ammonium, pyridinium and phosphonium¹⁻³, have played an important role in the synthesis of organic compounds, chemical industry^{4, 5} and pharmacy⁶⁻⁹. There are a large number of reports on the synthesis of various types of quaternary salts which have many interesting properties including ease of synthesis, high thermal stability, solubility in water and organic solvents, such as methanol, acetone, dichloromethane and chloroform, electrochemical durability, high viscosity, very low vapor pressure, and long shelf life. Due to their individual properties, these quaternary organic salts are striking in field of organic chemistry as catalysts^{10, 11}, phase transfer catalysts^{12, 13}, halogenating agents¹⁴, oxidative^{15, 16} and reductive¹⁷ reagents in some organic reactions. Organic phosphonium salts are the structural analogs of organic ammonium salts, with expectedly similar chemical properties. Nevertheless, these reagents may react under milder conditions than organic ammonium tribromides. Our use of phosphonium salts rather than ammonium or imidazolium analogs is motivated by the fact that phosphorus atom has a larger atomic radius, a greater polarizability and a lower binding energy with anions than nitrogen atom. These attributes make phosphonium salts attractive and interesting alternative halogenation reagents. There are many different cations and their counterions that can be used as oxidative¹⁸, reductive or brominating agents in polar and non-polar solvents¹⁹. Considering the diverse uses of these reagents, it becomes important to incorporate newer tribromides into the existing series. Bromination of alkenes and aromatic substrates, is usually carried out by bromine solution, but organic ammonium and phosphonium tribromides are preferable since they do not have the hazards that are associated with liquid bromine and they are regioselective²⁰ and stereoselective²¹. Other advantages of organophosphorus tribromides are that they are crystalline, easy to handle and maintain the desired stoichiometry. These salts are sometimes used as a conveniently weighable, green, non-toxic solid source of bromine in organic synthesis. Therefore several tribromides have been synthesized. The most frequently used quaternary phosphonium tribromide reagents as efficient brominating agents are benzyltriphenyl phosphonium tribromide^{22, 23}, tridecylmethyl phosphonium tribromide²¹, ethyltriphenyl phosphonium tribromide²⁴, 1,2-ethanedylbis(triphenylphosphonium) ditribromide²⁵ and methyltriphenylphosphonium tribromide²⁶.

The Hirshfeld surface analysis is a powerful tool for the consideration of intermolecular interactions²⁷ in the crystal. By means of Hirshfeld surface analysis all interaction types (hydrogen bonding, close and distant van der Waals contacts, C–H··· π interactions, π – π stacking) are readily identifiable and it becomes a straightforward method to classify molecular crystals by the nature of interactions when examining crystal packing diagrams.

We report herein the synthesis, characterization (¹H NMR, ¹³C NMR, ³¹P NMR, FT-IR, DSC and TG/DTG/DTA), single crystal X-Ray analysis and DFT calculations of 1,3-propanediylbis(triphenylphosphonium) dibromide **I** and 1,3-propanediylbis(triphenylphosphonium) monotribromide **II** as a green, mild, nontoxic and efficient brominating agent for double bonds and phenolic rings. By using specialized software (Crystal Explorer), we obtained Hirshfeld surfaces 3D maps and 2D fingerprint plots to explanation of intermolecular short contacts in the crystals. Furthermore, we report bromination of double bonds and phenolic rings with excellent yields at room temperature by the use of the title salt **II**.

Results and discussion

In the first step 1,3-propanediylbis(triphenylphosphonium) dibromide **I** was synthesized in refluxing DMF. The product was filtered and washed with DMF. The white powder was recrystallized in hot water (95 % yield). In the second step, the bromide salt **I** was treated dropwise with potassium tribromide in aqueous solution at room temperature in a 1:1 ratio. The yellow precipitate of **II** was formed, filtered and dried overnight under stream of air (97 % yield) (Scheme 1).



Scheme 1. Synthesis of 1,3-propanediylbis(triphenylphosphonium) bromide **I** and monotribromide **II**

Crystal structure description

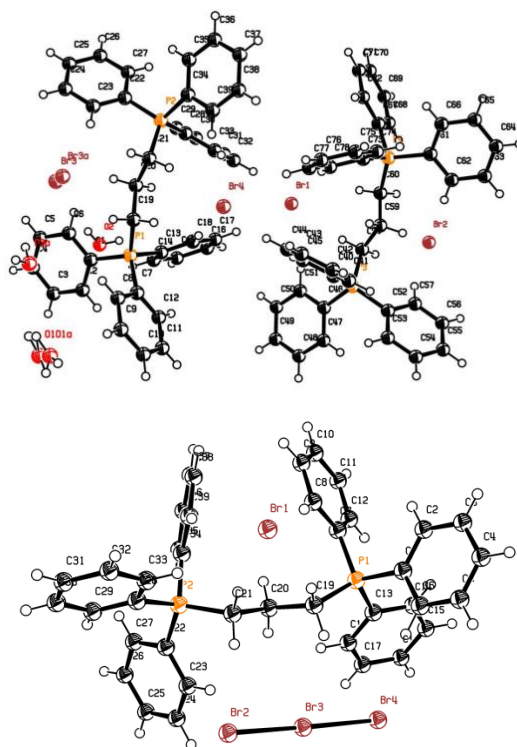
Based on the results of single crystal X-ray analysis of **I**, this compound crystallizes in the monoclinic system having chiral $P2_1$ space group with $Z = 4$. The asymmetric unit contains two independent molecules of triphenyl phosphonium cations, four bromide anions (1:2 ratio of cationic to anionic units) and three water molecules. The positional disorders were observed for one of four bromide anions (Br3) and oxygen atom of water molecule (O1) with an occupancy ratio of 72.28 and 73.27 % for Br3 and O1 atoms, respectively. The ORTEP diagram of compound **I** is shown in Figure 1 (top). The cations located in general positions and the phosphorous atoms exhibit a slightly distorted tetrahedral geometry. The bond angles around the P atoms are in the range of 107.0(2)° to 113.8(3)° for P₁, 106.2(2)° to 111.4(2)° for P₂, 107.5(2)° to 111.6(3)° for P₃ and 107.2(2)° to 113.1(3)° for P₄. The geometry of dications (bond lengths and angles) is general and comparable with our previously reported structures^{25, 28, 29}. The 3D

supramolecular network of this compound is dominated by the variety of C-H \cdots Br, O-H \cdots Br and C-H \cdots O hydrogen bonds (Figure 2), as well as C-H \cdots π interactions which can play a crucial role in the stabilization of supramolecular assemblies (Figure 3 top). Hydrogen bond geometry parameters are tabulated in supporting information file, Table S10.

In the crystal packing of **I**, the bistriphenylphosphonium dication and bromide anion are linked together by several C-H \cdots Br hydrogen bonds with H \cdots Br distances ranging from 2.697 to 3.134 Å. The water molecules are involved in the hydrogen bond interactions with the anion via O-H \cdots Br interactions (Figure 2). The cation moieties also interact through C-H \cdots π interactions with each other. As expected, the bromide anion in **I** inserts into the 1D chain of bistriphenylphosphonium dications in which each cation alternately links anion and solvent molecules together (Figure 3, top). Overall, the interaction results in supramolecular network of ionic moieties producing the three dimensional pattern.

The monotribromide compound **II** crystallizes in the monoclinic system with $P2_1/c$ space group with $Z = 4$. The asymmetric unit of this compound includes one triphenyl phosphonium cation, one bromide ion and one tribromide ion. Interestingly, there are two different anions (Br^- and Br_3^-) in the crystal packing of **II** (Figure 3 down). The ORTEP diagram of compound **II** is shown in Figure 1 (down). Similar to **I**, the structure of the cationic unit shows the distorted tetrahedral geometry for phosphorous atoms. The bond angles around the P atoms are in the range of 106.5(3)° to 113.8(4)° for P_1 and 105.9(2)° to 112.3(2)° for P_2 . Investigation of crystal packing structure of **II** revealed that C-H \cdots Br hydrogen bonds are dominant interaction in the stabilization of supramolecular architecture. In this structure, the bistriphenylphosphonium dication and tribromide anion are linked together by several C-H \cdots Br hydrogen bonds with H \cdots Br distances ranging from 2.830 to 3.171 Å for Br_3^- and 2.636 to 3.109 Å for Br^- . Interestingly, the arrangement of cationic units in the crystal packing of **II** is similar to **I**. Tribromide anion in **II** was replaced with one of bromide anions and solvent molecules. (Figure 3, down). **Surprisingly, bromide anion formed the hepta-furcated hydrogen bonds as one Br^- acceptor and seven C-H donor moieties (Figure 4).**

Comparison of titled compounds indicated that changing accompanying anionic moiety from bromide to tribromide affects directional interactions between anionic and cationic units and therefore different supramolecular aggregation can be observed for these structures. In addition, the presence of solvent molecule in **I** resulted in the various solvent-based interactions, such as O-H \cdots Br and C-H \cdots O hydrogen bonds. One of the main interactions in these compounds are C-H \cdots π interactions which play a crucial role in their molecular aggregation in all crystallographic directions.



Figures 1. The ORTEP diagram of compound **I** (top) and compound **II** (down) with 50% probability displacement ellipsoids and atom numbering (hydrogen atoms numberings are omitted for more clarity). **There are positional disorders for the bromide anion Br^- (Br3) and oxygen atom of water molecule (O1) in compound **I** with an occupancy ratio of 72.28 and 73.27 %, respectively.**

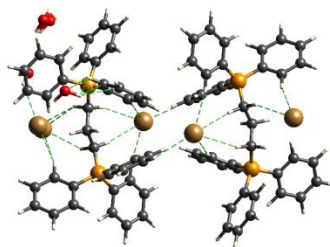
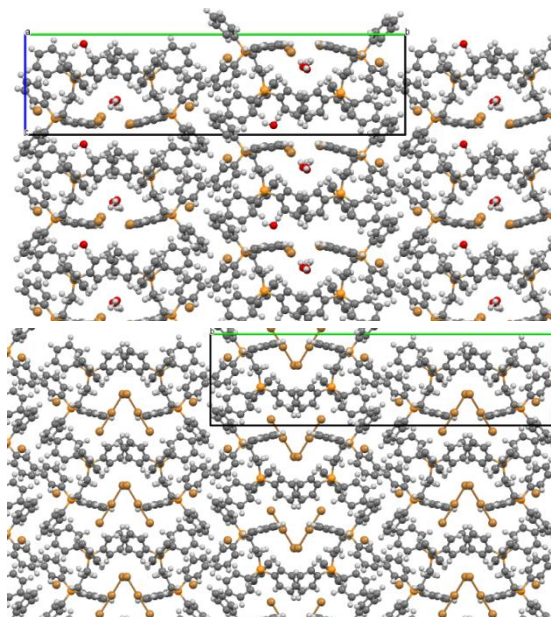


Figure 2. Hydrogen bonds in compound **I**



Figures 3. Presentation of crystal packing structures of compound **I** (top) and **II** (down) along a and c crystallography axis, respectively

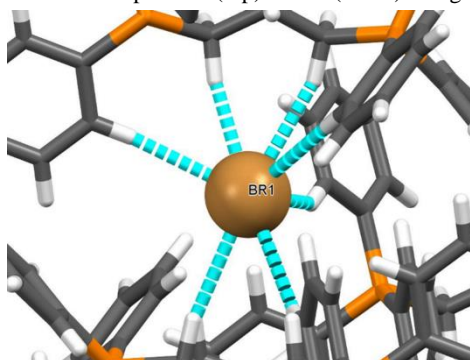


Figure 4. Presentation of heptafurcated hydrogen bonds comprised of one Br⁻ acceptor and seven C-H donor moieties in compound **II**

Thermal properties of salts **I and **II****

DSC thermograms have been recorded under nitrogen purging (50 mL/min.). The thermogram of compound **I** shows an endothermic sharp peak at 349-353 °C due to melting point and unsymmetrical low and broad peaks in the range of 360-380 °C assigned to decomposition of **I** (Figure 5).

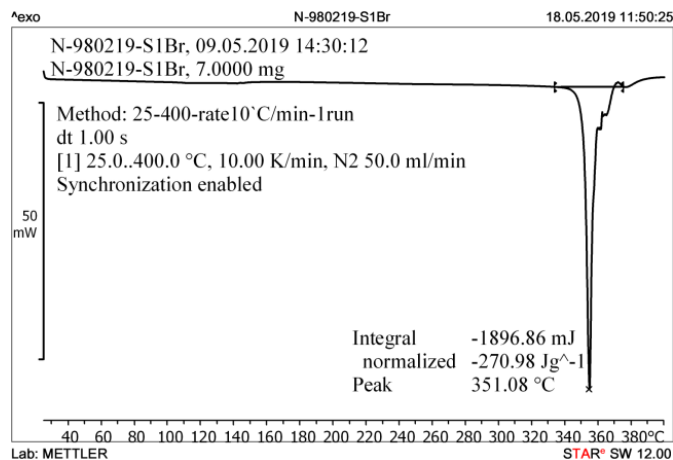


Figure 5. DSC thermogram of compound **I**

An endothermic sharp peak at 163-166 °C due to melting point, a broad exothermic peak at 270-330 °C and a broad endothermic peak at 330-380 °C assigned to decomposition of anion and cation, respectively are observable in the thermogram of compound **II** (Figure 6).

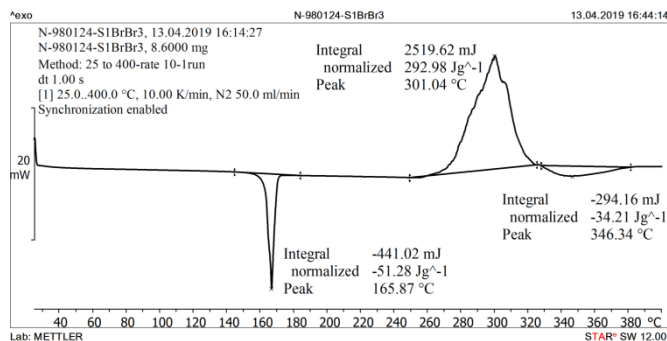


Figure 6. DSC thermogram of compound **II**

In the TG/DTG/DTA thermogram of **I**, an endothermic peak at 350 °C assigned to melting point is observed in the DTA blue curve with a small decrease in the TG red curve (by about 3-4 %) due to evaporation of water molecules. Immediately after that peak, a broad endothermic shoulder peak with a sharp and significant decrease in the TG curve has been recorded in the DTA curve (more than 90 %) assigned to decomposition of **I**. Ultimately, there is a broad endothermic peak in the range of 350-380 °C in the DTG brown curve due to decomposition of **I** (Figure 7).

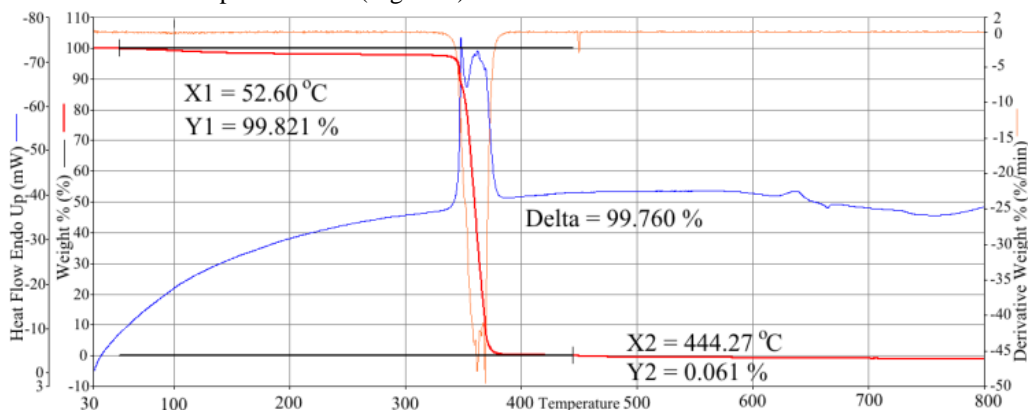


Figure 7. TG/ DTG/ DTA thermogram of compound **I**

The thermogram for **II** shows an endothermic sharp peak at about 165 °C in the DTA blue curve and the smallest decrease in the TG red curve (1 %) for melting point. The broad endothermic peak in the range of 320-370 °C in the DTA curve, a strong broad peak in DTG brown curve assigned to decomposition of compound **II** and about 7.7 % at 800 °C in TG red curve for remaining ash were observed (Figure 8). The DSC and TG/DTG/DTA thermograms show that compound **I** is more thermally stable than compound **II**. However, both salts are very stable on the bench-top in solid form or in solution of organic solvent and in contact with air without any change in color or performance over 6 months.

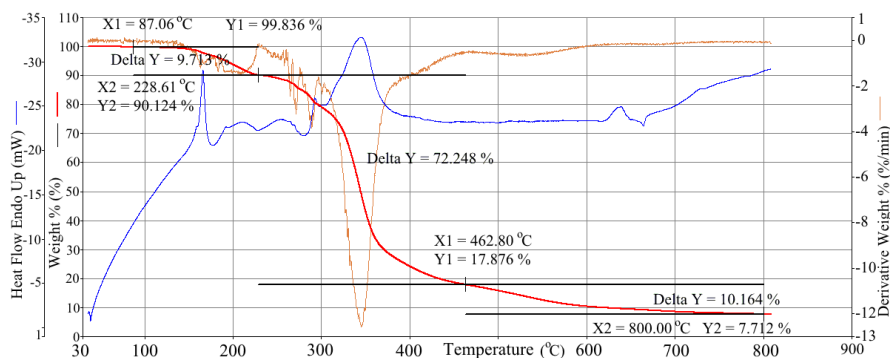


Figure 8. TG/ DTG/ DTA thermogram of compound **II**

Computational studies

The theoretical calculations were performed by using the Gaussian 09 software package, at the DFT-B3LYP level and with 6-311+G* basis sets for compound **I**, as well as compound **II**.

The bond lengths, bond angles and dihedral (torsion) angles were compared with X-ray crystallographic data. The calculation shows a good correlation between the theoretical and SC-XRD experimental structural parameters of compounds (See supporting information file).

Natural charge distribution on the molecules of **I** and **II** were calculated by NBO method. Calculations showed that P and H atoms have positive character while C and Br atoms have negative ones (Tables S4 and S5).

The interaction between the frontier molecular orbitals (HOMO from one molecule and LUMO from the other) is an important part of the total orbital interaction between two molecules. This interaction can only occur if the orbitals have the correct symmetry. The strength of the interaction is directly related to the HOMO-LUMO energy separation. In general, the smaller the HOMO-LUMO separation, the stronger the interaction and the more favored the reaction becomes³⁰. The energy level of the HOMO orbital shows tendency toward giving an electron as a donor in reactions while the energy level of LUMO orbital shows the ability to taking an electron as acceptor. HOMO-LUMO energies and the energy gap were calculated by B3LYP/ 6-311+G* presented in figures 9 and 10. Calculations indicate that although replacement of bromide by tribromide does not have any significant change in LUMO energy level, but it decreases the HOMO energy level (From -4.4585 eV to -4.8447 eV) and increases the HOMO-LUMO energy gap (From 2.3837 eV to 2.7725 eV) and consequently stabilizes the tribromide salt (For energy levels and energy gaps for **I** and **II** see figures S50 and S51).

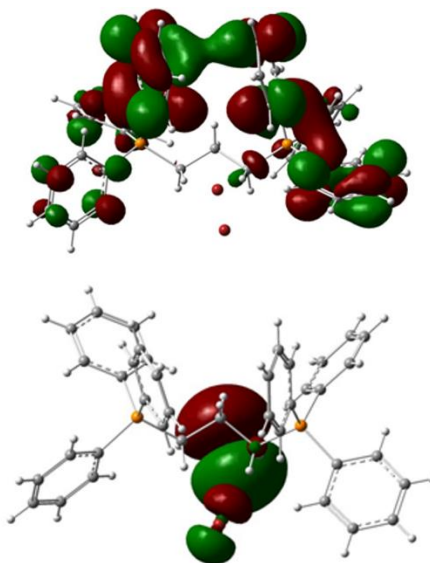


Figure 9. HOMO (down) and LUMO (top) diagrams for **I**

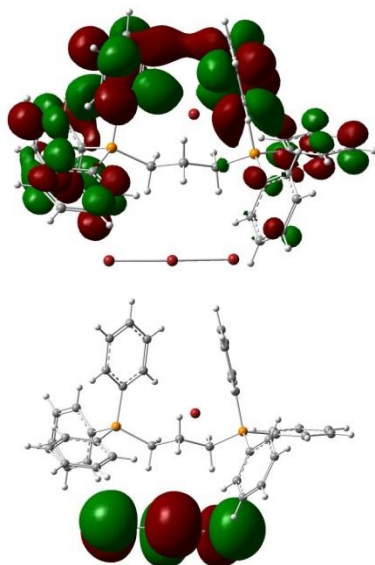


Figure 10. HOMO (down) and LUMO (top) diagrams for **II**

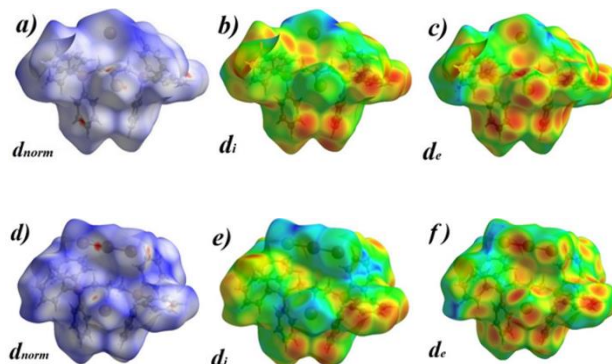
The Hirshfeld surface analysis

In order to visualize, quantify and explore the various intermolecular interactions of molecule in the crystal lattice of both compounds, Hirshfeld surfaces (HSs) and their associated 2D fingerprint plots (FPs) were calculated using Crystal Explorer 3.1 based on results of SC-X-ray analysis data^{28, 31}.

The function d_{norm} is a ratio consisting of the d_i (distance from the point to the nearest nucleus internal to the any Hirshfeld surface) and d_e (distance from the point to the nearest nucleus external to the surface) and the van der Waals (vdW) radii of the atoms. d_{norm} is a normalized contact distance, which is enable to identification of the regions of particular importance to intermolecular interactions in the crystal.

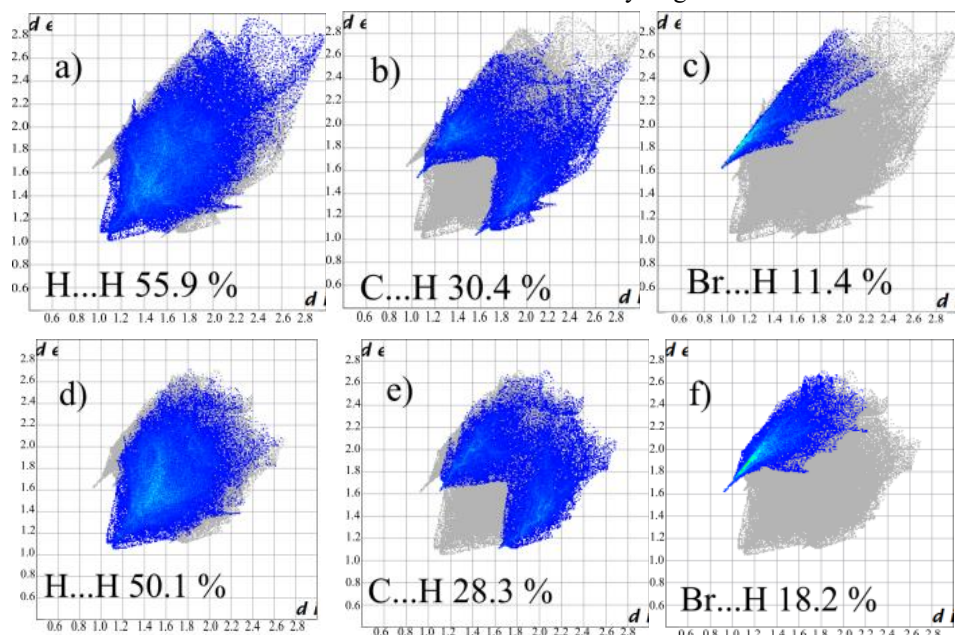
$$d_{norm} = \frac{d_i - r_i^{vdW}}{r_i^{vdW}} + \frac{d_e - d_e^{vdW}}{d_e^{vdW}}$$

The value of the d_{norm} is negative or positive when intermolecular contacts are, respectively, shorter or longer than vdW radii of the atoms. The d_{norm} values are mapped onto the Hirshfeld surface using a red–blue–white color scheme: red areas correspond to closer contacts and negative d_{norm} value, the blue areas correspond to longer contacts and positive d_{norm} value and the white regions are those where the distance of contacts is exactly the vdW separation and with a d_{norm} value of zero²⁷. Hirshfeld surfaces mapped with d_{norm} ranging from $-0.1219 \text{ \AA}^\circ$ (red) to 2.0166 \AA° (blue) for **I** (Figure 11a) and ranging from $-0.1410 \text{ \AA}^\circ$ (red) to 1.1896 \AA° (blue) for **II** (Figure 11d) and with d_i ranging from 1.0238 \AA° (red) to 3.1738 \AA° (blue) for **I** (Figure 11b) and ranging from 1.0116 \AA° (red) to 2.7888 \AA° (blue) for **II** (Figure 11e) and mapped with d_e ranging from 1.0256 \AA° (red) to 2.9770 \AA° (blue) for **I** (Figure 11c) and ranging from 1.0120 \AA° (red) to 2.7395 \AA° (blue) for **II** (Figure 11f) are calculated and plotted using Crystal Explorer software. Hirshfeld surface area of compounds **I** and **II** mapped with d_{norm} shows violent red spots on the surface near the Br ions which are due to $\text{Br}_{\text{inside}} \cdots \text{H}_{\text{outside}}$ contacts and violent red spots near the some of hydrogen atoms of aromatic rings and aliphatic chain near the surface in molecule which are due to $\text{H}_{\text{inside}} \cdots \text{Br}_{\text{outside}}$ contacts in the crystal structures (Figures 11a and 11d). The phosphorus atoms show no contacts in the crystal packing, as would be expected given their tetrahedral coordination. It can therefore be seen that the supramolecular architectures of **I** and **II** are mainly controlled by interactions between H and Br atoms.



Figures 11. Hirshfeld surfaces mapped with d_{norm} for the compound **I** (a) and **II** (d), mapped with d_i for the compound **I** (b) and **II** (e) and mapped with d_e for the compound **I** (c) and **II** (f)

A plot of d_i versus d_e is a 2D fingerprint plot which recognizes the existence and amount of different type of intermolecular interactions. The combination of d_e and d_i in the form of a 2D fingerprint plot provides summary of intermolecular contacts in the crystal. The relative contribution of different interactions to the Hirshfeld surface indicates that in cationic unit of compound **I**, the H...H (55.9 %), C...H (30.4 %) and Br...H (11.4 %) contacts account for about 97.7 % of the total Hirshfeld surface area and Br...C, Br...Br and C...C have very little effect on crystal packing. In cationic unit of compound **II**, the H...H (50.1 %), C...H (28.3 %) and Br...H (18.2 %) are main contacts about 96.6 % of total surface area and other contacts have no any considerable contribution in total Hirshfeld surfaces in the cation (Figures 12). By comparison, tribromide anion could affect the relative contribution of interactions and decreases the H...H while increases the Br...H hydrogen bonds in **II**.



Figures 12. 2D fingerprint plots for main close contact contributions (in %) in Hirshfeld surface area for a) H...H b) C...H/H...C and c) Br...H/H...Br for compound **I** cation, d) H...H e) C...H/H...C and f) Br...H/H...Br for compound **II** cation

The analysis of the 2D finger print plot of cation **I** shows that Br...H and C...H contacts include 41.8 % of total Hirshfeld surface area as characteristic wings of the plot and most surface area belongs to H...H contacts with 55.9 % of total surfaces and also in cation **II** the Br...H and C...H contacts include 46.5 % of total Hirshfeld surface area as characteristic wings of the plot and most surface area belongs to H...H contacts with 50.1 % of total surfaces.

It is clearly observable that in 2D fingerprint plots of both cations, H...H interactions are most surface area and maximum interactions in crystal packing. The $\pi\cdots\pi$ contacts are almost zero, and there are no significant Br...Br interactions in the crystal structure of cations **I** or **II**. Chart 1 versus chart 2.

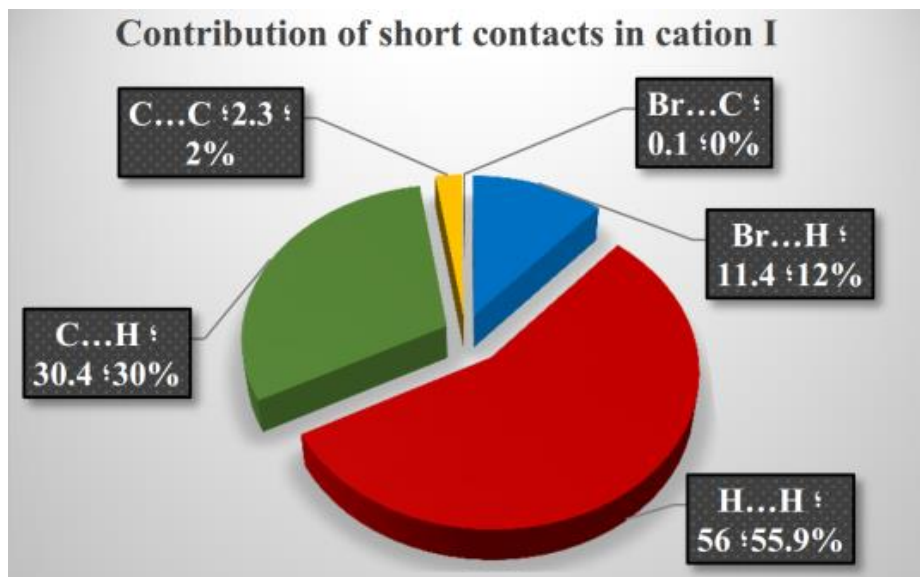


Chart 1. Percentage contribution of short contacts in the cation of compound **I**

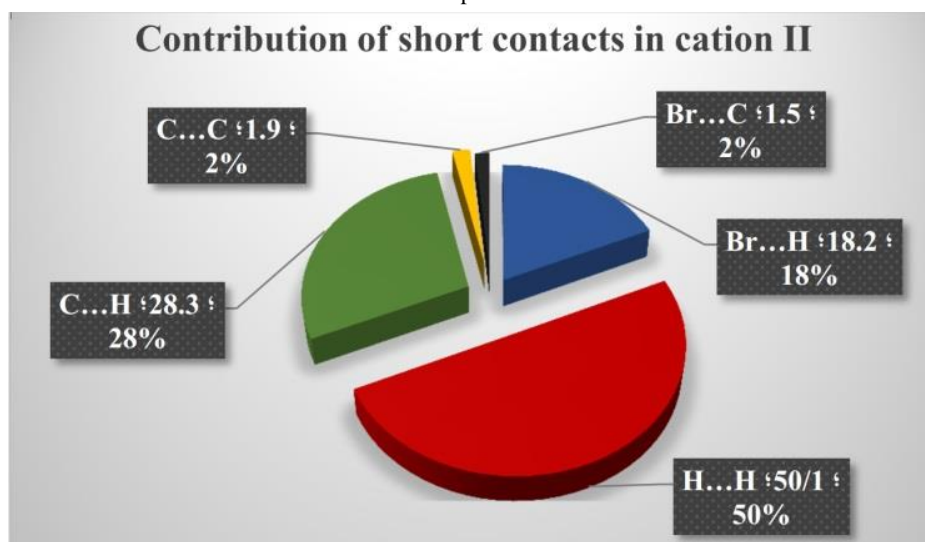


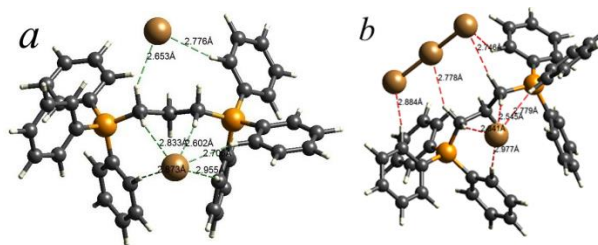
Chart 2. Percentage contribution of short contacts in the cation of compound **II**

The molecule **I** in the unit cell is connected by weak Br...H interactions between nearest neighbors. Nearest intramolecular interactions are Br₂...H_{21A} in 2.602 Å, Br₁...H_{19A} in 2.653 Å and Br₂...H₃₉ in 2.706 Å. Nearest intramolecular interactions in **II** are Br₁...H_{21A} in 2.545 Å, Br₂...H_{21B} in 2.746 Å and Br₃...H_{19A} in 2.778 Å (Figures 13). Nearest intramolecular interactions < 3 Å for **I** and **II** are tabulated in Table 1.

Since, the tribromide anion has three bromine atoms as good acceptors to interact with the other hydrogen bond donors, it can be predicted that the participation of Br...H contacts in the Hirshfeld surface area for **II** is higher than **I**.

Table 1. Nearest close contacts in **I** and **II**

	Compound I	<i>d</i> in Å	Compound II	<i>d</i> in Å
1	Br ₂ ...H _{21A}	2.602	Br ₁ ...H _{21A}	2.545
2	Br ₁ ...H _{19A}	2.653	Br ₂ ...H _{21B}	2.746
3	Br ₂ ...H ₃₉	2.706	Br ₃ ...H _{19A}	2.778
4	Br ₁ ...H ₂₃	2.776	Br ₁ ...H ₃₃	2.779
5	Br ₂ ...H _{19B}	2.833	Br ₁ ...H _{19B}	2.841
6	Br ₂ ...H ₁₈	2.873	Br ₂ ...H ₂₃	2.847
7	Br ₂ ...H ₃₃	2.955	Br ₄ ...H ₆	2.884
8			Br ₁ ...H ₈	2.977



Figures 13. a) Nearest close contacts in **I** and b) nearest close contacts in **II**

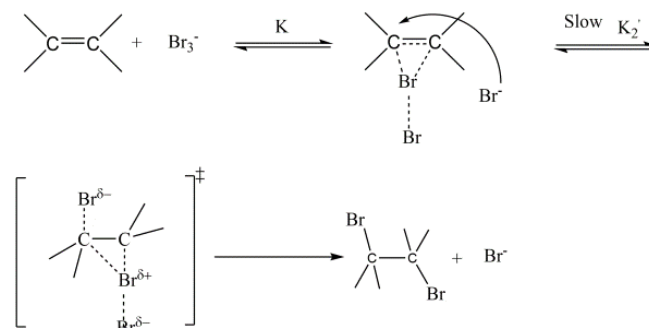
In addition to HS's and fingerprint plots, the quantitative measurements of HS's show that the molecular volume and surface area of **II** are bigger than **I** because of tribromide anion and the globularity of both compounds are nearly same whereas the asphericity of **I** is bigger than **II**. Significantly the molecular volume and surface area of cation **I** are bigger than cation **II** because of tribromide anion can collect the cation and cause the globularity of cation **II** to become bigger than cation **I** whereas asphericity of both cations are nearly same (Table 2).

Table 2. Quantitative measures of Hirshfeld surfaces for the compound **I** and **II** and their cations

Quantitative measures of Hirshfeld surfaces	molecular volume (V_H) \AA^3	surface area (S_H) \AA^2	globularity (G)	asphericity (Ω):
Compound I	845.07	626.98	0.689	0.061
Compound II	875.96	644.40	0.687	0.045
Compound I cation	750.53	598.96	0.667	0.087
Compound II cation	722.80	571.79	0.681	0.088

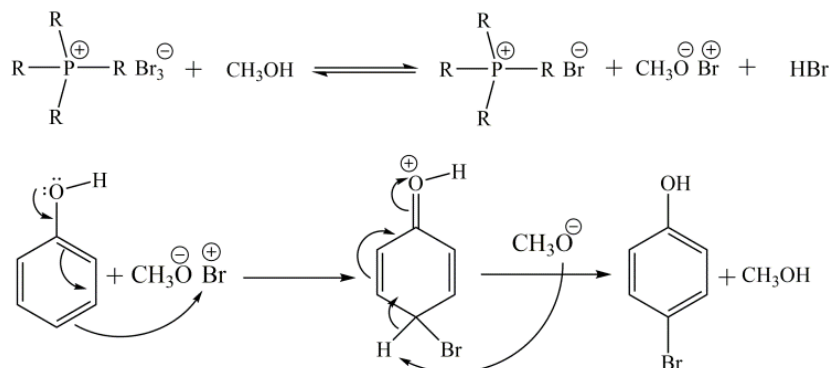
Bromination of alkenes and phenols

The bromination of double bonds and phenolic rings³² can be carried out by bromine or by organic tribromide salts but the mechanisms, thermodynamics and kinetics of the two reactions are different³³. Bromination of alkenes (cyclohexene in 1,2-dichloroethane) has a negative entropy ($\Delta S^\ddagger = -40.9$ eu), a positive enthalpy ($\Delta H^\ddagger = +6.0$ kcal/mol) and a positive activation energy ($E_a = +6.6$ kcal/mol). The proposed mechanism for the bromination of alkenes is presented in Scheme 2.



Scheme 2. Proposed mechanism for bromination of alkenes with tribromide anion

A plausible mechanism for bromination of phenolic compounds in the mixed solvent system ($\text{CH}_2\text{Cl}_2/\text{MeOH}$, 1:1) can be outlined in Scheme 3^{25, 32}.



Scheme 3. Proposed mechanism for bromination of phenolic compounds with tribromide anion

In our work, the bromination of double bonds and phenolic compounds was carried out by using organic tribromide **II** in dichloromethane and dichloromethane/methanol solvent system at room temperature. Both electron withdrawing and electron donating groups were placed on the double bond and phenolic ring to investigate the substituents effect on the rate of reactions. It was found that substituents significantly influenced the reaction time. In general, bromination of alkenes proceeded in good yields, but electron withdrawing groups, such as nitro group, increased the reaction time and decreased the reaction yields. Also for phenolic compounds, electron withdrawing groups, such as nitro and chloro groups increased the reaction time and decreased reaction yields, and electron donating groups, such as methyl group decreased reaction time and increased reaction yields. (Table S8 and S9).

Conclusion

In conclusion, the present paper describes the synthesis and characterization of two quaternary phosphonium salts. The crystal structure, the DFT calculations, analysis of Hirshfeld surfaces and fingerprint plots, as well as spectroscopic properties (^1H , ^{13}C , ^{31}P NMR, FT-IR) and thermal behavior of the salts (by DSC-TG/DTA) were studied and reported. Furthermore, the tribromide title salt was used as mild brominating and oxidizing agent to selective bromination of C-C double bonds and phenolic rings, instead of very active, non-selective and toxic molecular bromine.

Experimental Section

Triphenylphosphine and potassium bromide were purified by recrystallization to obtain purity of 99.5 % in each case. The purity of *N,N*-dimethylformamide (99.7%) and dichloromethane (99.8%) was checked by GC. Water as a solvent was HPLC grade. The reaction progress was monitored by TLC and GC. NMR spectra were recorded by the Bruker AC spectrometer at 500 or 300 MHz (^1H NMR, compound **I** and **II**, respectively), 75 or 125 MHz (^{13}C NMR, compound **I** and **II**, respectively) and 200 MHz (^{31}P NMR for both compounds) using D_2O , $\text{DMSO-}d_6$ and CDCl_3 as solvents.

DSC thermograms recorded by METTLER TOLEDO DSC-1 instrument. TG/DTG/DTA thermograms were recorded by Perkin Elmer Diamond TG/DTA thermal analyzer. Melting and boiling points were determined by METTLER TOLEDO FP900 system, FP81 cell. Infrared spectra were recorded on a Perkin Elmer Spectrum 65-FT-IR spectrometer as KBr disks (4000- 400 cm^{-1} region). GLC analysis was performed with Agilent Technology 6890N Gas Chromatograph with a FID detector and cp-sil 5 CB 50 m, 0.32 mm, 1.2 μm capillary column. GC/MS spectra were recorded by Varian 3800 GC and Varian Saturn 2000 Ion trap as a detector and cp-sil 8 CB low bleed/MS 30 m, 0.25 mm, 0.25 μm capillary column.

Preparation of 1,3-propanediylbis(triphenylphosphonium) dibromide ($\text{C}_{39}\text{H}_{36}\text{P}_2\text{Br}_2$) **I**

A mixture of the triphenylphosphine (6.55 g, 25 mmol, excess) and 1,3-dibromopropane (2.01 g, 1.01 mL, 10 mmol, $d = 1.989 \text{ g/cm}^3$) in DMF (30 mL) was stirred and refluxed for 4 h. After reaction was complete, the reaction mixture was cooled and the crude white precipitate was filtered and washed with DMF ($3 \times 10 \text{ mL}$). The white powder was dried under stream of air and recrystallized in water as cubic shape crystals (6.9 g, 95 % yield) (Figure S47 in supporting information file), m.p. 349-353 $^\circ\text{C}$ (by DSC). Single-crystals of compound **I** were grown by slow evaporation of an aqueous solution at room temperature. ^1H NMR (500 MHz, D_2O , δ ; ppm): 1.90 (brs, 2H, C^{20}H_2), 3.55 (brs, 4H, $\text{C}^{19,21}\text{H}_2$), 7.67, 7.86 ($2 \times$ brs, 30H, $6 \times \text{C}_6\text{H}_5$). ^{13}C NMR (75 MHz, $\text{DMSO-}d_6$, δ ; ppm): 16.54(C20), 20.63 (C21, C19), 117.78, 118.93, 130.80, 134.09 and 135.52 ($5 \times$ s, C_6H_5). ^{31}P NMR (200 MHz, CDCl_3 , δ ; ppm): 35.69. FT-IR (KBr, $\bar{\nu}/\text{cm}^{-1}$): 537(s), 685, 723(s, C-H_{aromatic} bend), 993(m), 1108(s, C-P stretch), 1190(w), 1328(m), 1432(s, Ph-P stretch), 1482(m, C-H_{aliphatic} bend), 2801(w), 2865(m, C-H_{aliphatic} stretch), 3009(m, C-H_{aromatic} stretch). Elemental analyses (%): calcd.: C, 64.46; H, 4.95; Br, 22.03; found: C, 64.71; H, 4.79; Br, 22.24.

Preparation of 1,3-propanediylbis(triphenylphosphonium) monotribromide ($\text{C}_{39}\text{H}_{36}\text{P}_2\text{Br}_4$) **II**

Bromine (1.03 mL, 20 mmol) was added dropwise to a mixing solution of KBr (2.38 g, 20 mmol) in H_2O (30 mL). Bromine layer dissolved after 30 min. The KBr_3 solution was added to the aqueous solution of 1,3-propanediylbis(triphenylphosphonium) dibromide **I** (7.26 g, 10 mmol in 20 mL of water). The solution was mixed for over 30 min. The yellow precipitate was filtered and washed with cooled water ($3 \times 10 \text{ mL}$). The product was air-dried overnight and recrystallized in CH_2Cl_2 as needle shape crystals (97 % yields), (Figure S48 in supporting information file), m.p. 163-166 $^\circ\text{C}$ (by DSC). Single-crystals of compound **II** were grown by slow evaporation of dichloromethane solution at room temperature. ^1H NMR (300 MHz, $\text{DMSO-}d_6$, δ ; ppm): 1.80 (brs, 2H, C^{20}H_2), 3.88 (brs, 4H, $\text{C}^{19,21}\text{H}_2$), 7.82 (brs, 30H, $6 \times \text{C}_6\text{H}_5$). ^{13}C NMR (125 MHz, CDCl_3 , δ ; ppm): 16.38(s, C20), 22.49 (s, C21, C19), 115.58, 116.31, 129.89, 132.68 and 134.42 ($5 \times$ s, C_6H_5). ^{31}P NMR (200 MHz, CDCl_3 , δ ; ppm): 34.83 (s) for P atom. FT-IR (KBr, $\bar{\nu}/\text{cm}^{-1}$): 508.2(s), 539.7(s), 686.6(s), 721.8(s, C-H_{aromatic} bend), 994(m), 1111.2(s, C-P stretch), 1190.9(m), 1329.6(m), 1436.3(s, Ph-P stretch), 1484(m, C-H_{aliphatic} bend), 2803.8(m), 2867.8(m, C-H_{aliphatic} stretch), 3013.8(m, C-H_{aromatic} stretch). Elemental analyses (%): calcd.: C, 52.82; H, 4.06; Br, 36.11; found: C, 52.93; H, 4.21; Br, 35.92. ^1H NMR spectra of compounds **I** and **II** showed three distinctive peaks corresponding to carbon atoms of the center CH_2 , terminal CH_2 and aromatic groups in a ratio 1:2:15 respectively. The exchange of the bromide to the tribromide anion caused very little changes in chemical shifts (0.1 - 0.4 ppm in ^1H NMR and 0.8 ppm in ^{31}P NMR) (see SI).

Caution: Bromine is toxic, corrosive, and dangerous for the environment. Keep container tightly closed and in a well-ventilated place. In case of contact with eyes, rinse immediately with plenty of water and seek medical advice. In case of accident or if you feel unwell, seek medical advice immediately (show the label where possible). Avoid release to the environment.

General experimental procedure for bromination of alkenes

To a stirred mixture of alkene (3 mmol) in dichloromethane (5 mL) was added solution of 1,3-propanediylbis(triphenylphosphonium) mono tribromide **II** (3 mmol) in dichloromethane (5 mL) at room temperature. The reaction progress was monitored by TLC and GC. After disappearance of the yellow-orange color of reagent **II**, the solvent was evaporated and diethyl ether was added (3 × 5 mL) for extraction. The mixture was filtered and the solvent was evaporated. The crude product was purified with column chromatography over silica gel (pore size 60 Å, 200-400 mesh particle size) using a mixture of n-hexane and ethyl acetate (8:2) as the eluent. The main products, reaction times and isolated yields are tabulated in Table S8. To confirm identity of the products, they were subjected to GC/MS analysis and their spectra were compared and validated with the NIST library (see SI). All of the isolated products are known and their physical data have been reported in literature³⁴.

General experimental procedure for bromination of phenolic rings

To a solution of phenolic compound (3 mmol) in dichloromethane/methanol 50 % (5 mL) was added 1,3-propanediylbis(triphenylphosphonium) monotribromide **II** (3 mmol) in dichloromethane (5 mL) at room temperature. The reaction progress was monitored by TLC and GC. After disappearance of the yellow-orange color of reagent **II**, the solvent was evaporated. The extraction was carried out with diethyl ether (3 × 5 mL). The mixture was filtered and the solvent was evaporated. The crude product was purified with column chromatography over silica gel (pore size 60 Å, 200-400 mesh particle size) using a mixture of n-hexane and ethyl acetate (8:2) as the eluent. The main products, reaction times and isolated yields are tabulated in Table S9. To confirm identity of the products, they were subjected to GC/MS analysis and their spectra were compared and validated with NIST library (see SI). All of the isolated products are known and their physical data have been reported in literature³⁴.

X-ray crystallography analysis

X-ray diffraction experiments on **I** and **II** were carried out at 100(2) K on a Bruker APEX II diffractometer using Mo-K α radiation ($\lambda = 0.71073$ Å). Data collections were performed using a CCD area detector from a single crystal mounted on a glass fibre. Intensities were integrated in SAINT and absorption corrections based on equivalent reflections were applied using SADABS³⁵. Both of the structures, **I** and **II** were solved using ShelXT³⁶ and refined by full matrix least squares against F^2 in ShelXL^{37, 38}, using Olex2³⁹. All of the non-hydrogen atoms were refined anisotropically, while all of the hydrogen atoms were located geometrically and refined using a riding model. **One of the bromide anions (Br3)** and oxygen atom of water molecule (O1) in compound **I** showed the positional disorder and were refined with an occupancy ratio of 72.28 and 73.27 for these atoms, respectively. The structural resolution procedure was performed using WinGX crystallographic software package⁴⁰. Crystal structure and refinement data are given in Table 3. CCDC 1947472-1947473 contains the supplementary crystallographic data for this paper. These data can be obtained free of charge via www.ccdc.cam.ac.uk/retrieving.html (or from the Cambridge Crystallographic Data Centre 12, Union Road, Cambridge, B2 1EZ; UK, fax +441223336033; or deposit@ccdc.cam.ac.uk).

Table 3. Crystal data and structure refinement for **I** and **II**

Identification code	I	II
Empirical formula	C ₃₉ H ₃₆ P ₂ Br ₂ .H _{2.66} O _{1.33}	C ₃₉ H ₃₆ P ₂ Br ₄
Formula weight	750.44	886.26
Temperature/K	100(2)	100(2)
Crystal system	monoclinic	monoclinic
Space group	$P2_1$	$P2_1/c$
$a/\text{Å}$	9.3070(3)	10.3701(3)
$b/\text{Å}$	37.3087(11)	37.4291(12)
$c/\text{Å}$	10.2239(4)	9.4941(3)
$\alpha/^\circ$	90	90

$\beta/^\circ$	105.750(2)	105.725(2)
$\gamma/^\circ$	90	90
Volume/ \AA^3	3416.8(2)	3547.15(19)
Z	4	4
$\rho_{\text{calc}}/\text{cm}^3$	1.459	1.660
μ/mm^{-1}	2.498	4.656
F(000)	1533.0	1760.0
Radiation	Mo-K α ($\lambda = 0.71073$)	Mo-K α ($\lambda = 0.71073$)
2 θ range for data collection/ $^\circ$	4.14 to 55.824	4.08 to 55.836
Index ranges	$-11 \leq h \leq 12, -49 \leq k \leq 49, -13 \leq l \leq 12$	$-13 \leq h \leq 13, -44 \leq k \leq 49, -12 \leq l \leq 12$
Reflections collected	63046	31917
Data/restraints/parameters	16316/1/818	8500/0/406
Goodness-of-fit on F^2	1.059	1.021
Final R indexes [$I > 2\sigma(I)$]	$R_1 = 0.0348, wR_2 = 0.0658$	$R_1 = 0.0346, wR_2 = 0.0663$
Final R indexes [all data]	$R_1 = 0.0405, wR_2 = 0.0672$	$R_1 = 0.0530, wR_2 = 0.0709$
Largest diff. peak/hole / $e \text{\AA}^{-3}$	0.74/-0.46	1.83/-0.78

ASSOCIATED CONTENT

Supporting Information

Copies of NMR spectra, GC chromatograms, GC/MS spectra, FT-IR spectra, DSC and TG/DTA thermograms, X-Ray crystallography data, computational studies results

X-ray crystallography data of compounds **I** and **II** (CIF)

The supporting Information is available free of charge on the ACS publications website at DOI:

AUTHOR INFORMATION

Corresponding Author

*✉ (Mostafa Gholizadeh): m_gholizadeh@um.ac.ir

Acknowledgments

We are grateful for partial support of this work (Grant number 3/45675) by Ferdowsi University of Mashhad Research Council. The authors would like to specially thank Petrochemical Research and Technology Co to provide DSC Thermograms, GC Chromatograms and Mass spectra.

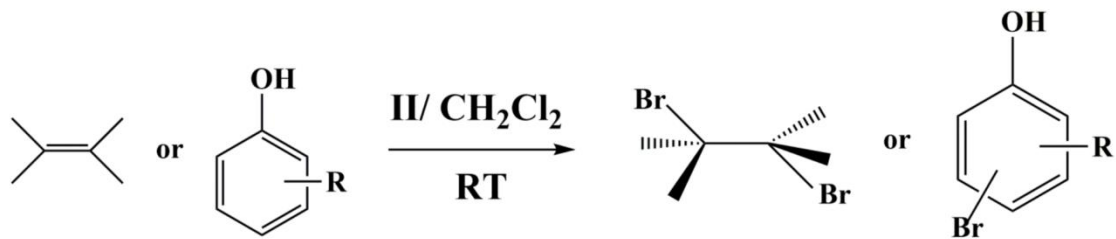
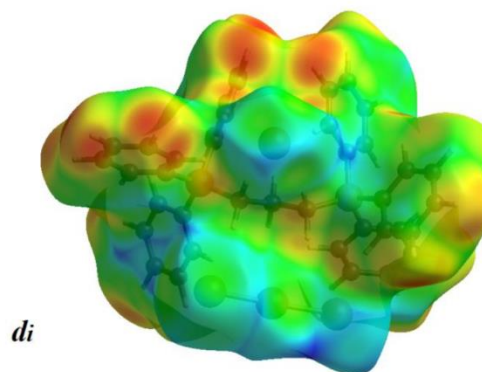
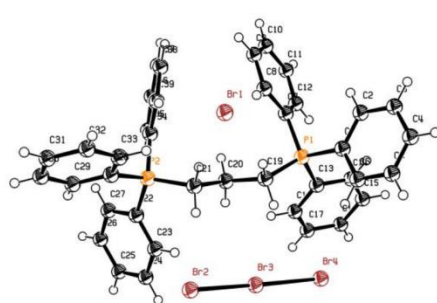
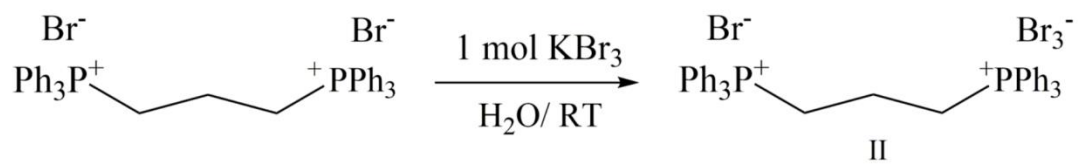
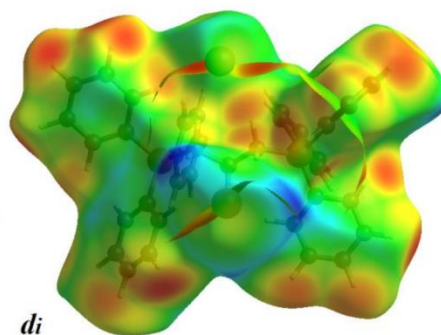
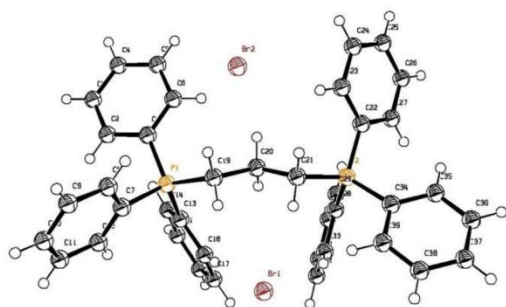
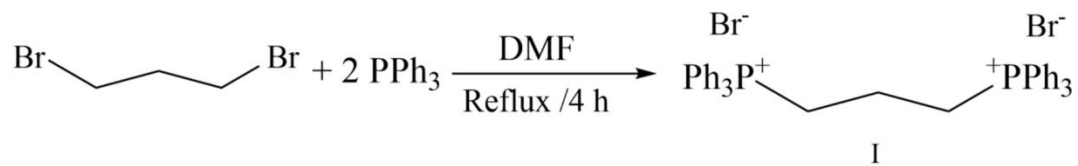
References

(1) C. Chiappe, Ionic Liquids in Organic Synthesis: Effects on Rate and Selectivity, (2008), 265-568,

- (2)K. Ghandi, A review of ionic liquids, their limits and applications, *Green and sustainable chemistry*, **(2014)**, 01, 4, 44-53
- (3)M. A. B. Zahoor Ullah, Zakaria Man and Amir Sada Khan Phosphonium-based ionic liquids and their application in separation of dye from aqueous solution, *ARPN Journal of Engineering and Applied Sciences*, **(2016)**, 3, 11, 1653-9
- (4)J. Castillo, M. T. Coll, A. Fortuny, P. N. Donoso, R. Sepúlveda and A. M. Sastre, Cu (II) extraction using quaternary ammonium and quaternary phosphonium based ionic liquid, *Hydrometallurgy*, **(2014)**, 141, 89-96
- (5)M. Rzelewska, M. Janiszewska and M. Regel-Rosocka, Application of quaternary phosphonium salts as extractants of Ru (III) and Rh (III) from model aqueous solutions, *Chemik*, **(2016)**, 9, 70, 515-20
- (6)B. Bachowska, J. Kazmierczak-Baranska, M. Cieslak, B. Nawrot, D. Szczesna, J. Skalik and P. Balczewski, High Cytotoxic Activity of Phosphonium Salts and Their Complementary Selectivity towards HeLa and K562 Cancer Cells: Identification of Tri-n-butyl-n-hexadecylphosphonium bromide as a Highly Potent Anti-HeLa Phosphonium Salt, *ChemistryOpen*, **(2012)**, 1, 1, 33-8
- (7)E. Gazzano, L. Lazzarato, B. Rolando, J. Kopecka, S. Guglielmo, C. Costamagna, K. Chegaev and C. Riganti, Mitochondrial Delivery of Phenol Substructure Triggers Mitochondrial Depolarization and Apoptosis of Cancer Cells, *Frontiers in pharmacology*, **(2018)**, 9, 580-
- (8)Y. Xue, H. Xiao and Y. Zhang, Antimicrobial polymeric materials with quaternary ammonium and phosphonium salts, *International journal of molecular sciences*, **(2015)**, 2, 16, 3626-55
- (9)Y. Xue, Y. Pan, H. Xiao and Y. Zhao, Novel quaternary phosphonium-type cationic polyacrylamide and elucidation of dual-functional antibacterial/antiviral activity, *RSC Advances*, **(2014)**, 87, 4, 46887-95
- (10)T. Werner, Phosphonium salt organocatalysis, *Advanced synthesis & catalysis*, **(2009)**, 10, 351, 1469-81
- (11)F. Shirini, M. S. Langroodi and M. Abedini, Efficient synthesis of bis (indolyl) methanes catalyzed by (PhCH₂PPh₃)⁺ Br₃⁻ under solvent-free conditions, *Chinese Chemical Letters*, **(2010)**, 11, 21, 1342-5
- (12)T. Chang, H. Jing, L. Jin and W. Qiu, Quaternary onium tribromide catalyzed cyclic carbonate synthesis from carbon dioxide and epoxides, *Journal of Molecular Catalysis A: Chemical*, **(2007)**, 1-2, 264, 241-7
- (13)C. M. Starks, Phase-transfer catalysis. I. Heterogeneous reactions involving anion transfer by quaternary ammonium and phosphonium salts, *Journal of the American Chemical Society*, **(1971)**, 1, 93, 195-9
- (14)R. Cristiano, K. Ma, G. Pottanat and R. G. Weiss, Tetraalkylphosphonium Trihalides. Room Temperature Ionic Liquids As Halogenation Reagents, *The Journal of organic chemistry*, **(2009)**, 23, 74, 9027-33
- (15)R. Badri and A. Mostoufi, The synthesis and application of 3,6-bis(triphenylphosphonium) cyclohexene dichromate: An efficient oxidizing agent, *Phosphorus, Sulfur, and Silicon*, **(2006)**, 7, 181, 1513-9
- (16)R. Badri, H. Shalhaf and M. Heidary, 3,6-Bis(triphenylphosphonium)-cyclohexene peroxodisulfate: a highly efficient oxidant for the selective oxidation of benzylic alcohols, *Synthetic communications*, **(2001)**, 22, 31, 3473-9
- (17)H. Firouzabadi and M. Adibi, Methyltriphenylphosphonium tetrahydroborate (MePh₃PBH₄). A stable, selective and versatile reducing agent, *Phosphorus, Sulfur, and Silicon and the Related Elements*, **(1998)**, 1, 142, 125-47
- (18)R. Badri and M. Soleymani, 3, 6-bis (triphenylphosphonium) cyclohexene peroxodisulfate as an efficient and mild oxidizing agent for conversion of alkylbenzenes to corresponding carbonyl compounds, *Synthetic communications*, **(2002)**, 15, 32, 2385-9
- (19)H.-J. Cristau, E. Torreilles, P. Morand and H. Christol, Les tribromures de phosphoniums. Agents de bromation de substrats organiques, *Phosphorus and sulfur and the related elements*, **(1985)**, 3, 25, 357-67
- (20)Z. Li, X. Sun, L. Wang, Y. Li and Y. Ma, Silica-supported quinolinium tribromide: a recoverable solid brominating reagent for regioselective monobromination of aromatic amines, *Journal of the Brazilian Chemical Society*, **(2010)**, 3, 21, 496-501
- (21)K. Ma and S. Li, Stereoselective bromination reactions using tridecylmethylphosphonium tribromide in a "Stacked" reactor, *Organic letters*, **(2008)**, 19, 10, 4155-8
- (22)D. Xin-teng and L. Guo-bin, Bromination of Anilines by Benzyltriphenylphosphonium Tribromide, *Synthetic communications*, **(1989)**, 7-8, 19, 1261-5
- (23)A. R. Hajipour, S. A. Pourmousavi and A. E. Ruoho, An efficient method for thioacetalization of carbonyl compounds in the presence of a catalytic amount of benzyltriphenylphosphonium tribromide under solvent-free conditions, *Phosphorus, Sulfur, and Silicon and the Related Elements*, **(2007)**, 5, 182, 921-37

- (24)L. Jamir, B. Alimenla, A. Kumar, D. Sinha and U. B. Sinha, Synthesis and reactivity studies of a new reagent, ethyltriphenylphosphonium tribromide, *Synthetic Communications*, (2010), 1, 41, 147-55
- (25)R. Salmasi, M. Gholizadeh, A. Salimi and J. C. Garrison, The synthesis of 1, 2-ethanediybis (triphenylphosphonium) ditribromide as a new brominating agent in the presence of solvents and under solvent-free conditions, *Journal of the Iranian Chemical Society*, (2016), 11, 13, 2019-28
- (26)R. Cristiano, A. D. Walls and R. G. Weiss, Sequential bromination reactions from beads with methyltriphenylphosphonium tribromide groups, *Journal of Physical Organic Chemistry*, (2010), 10, 23, 904-9
- (27)M. A. Spackman and D. Jayatilaka, Hirshfeld surface analysis, *CrystEngComm*, (2009), 1, 11, 19-32
- (28)R. Salmasi, A. Salimi, M. Gholizadeh, A. Abolghasempour and J. C. Garrison, Crystal structure and solid state computational (DFT/Hirshfeld surface) study for probing a new efficient and recyclable oxidation reagent, 1, 2-ethandiybis (triphenylphosphonium) peroxodisulfate dihydrate, *Phosphorus, Sulfur, and Silicon and the Related Elements*, (2016), 10, 191, 1380-7
- (29)S. R. Nokhbeh, M. Gholizadeh, A. Salimi and H. A. Sparkes, Crystal structure, characterization, Hirshfeld surface analysis and DFT studies of two [propane 3-bromo-1-(triphenyl phosphonium)] cations containing bromide (I) and tribromide (II) anions: The anion (II) as a new brominating agent for unsaturated compounds, *Journal of Molecular Structure*, (2019), 1195, 542-54
- (30)K. Houk, Generalized frontier orbitals of alkenes and dienes. Regioselectivity in Diels-Alder reactions, *Journal of the American Chemical Society*, (1973), 12, 95, 4092-4
- (31)W. Śmiszek-Lindert, A. Michta, A. Tyl, J. Małecki, E. Chelmecka and S. Maślanka, X-ray, Hirshfeld surface analysis, spectroscopic and DFT studies of PAHs: Fluoranthene and acenaphthene, *Journal of the Serbian Chemical Society*, (2015), 12, 80, 1489 -504
- (32)A. R. Hajipour, S. E. Mallakpour, H. Imanieh and S. A. Pourmousavi, A controlled and selective bromination of phenols by benzyltriphenylphosphonium tribromide, *Journal of Chemical Research*, (2002), 6, 272-5
- (33)G. Bellucci, R. Bianchini, R. Ambrosetti and G. Ingrosso, Comparison of molecular bromine and tribromide ion as brominating reagents. 1. Kinetic evidence for different mechanisms of addition to cyclohexene, *The Journal of organic chemistry*, (1985), 18, 50, 3313-8
- (34)J. Buckingham, S.M. Donaghy, *Dictionary of organic compounds: 5th ed.*, (1987), v. 1-5,
- (35)Bruker AXS area detector scaling and absorption correction, (2014/5),
- (36)G. Sheldrick, SHELXT - Integrated space-group and crystal-structure determination, *Acta Crystallographica Section A*, (2015), 1, 71, 3-8
- (37)G. Sheldrick, Crystal structure refinement with SHELXL, *Acta Crystallographica Section C*, (2015), 1, 71, 3-8
- (38)G. Sheldrick, A short history of SHELX, *Acta Crystallographica Section A*, (2008), 1, 64, 112-22
- (39)O. V. Dolomanov, L. J. Bourhis, R. J. Gildea, J. A. K. Howard and H. Puschmann, OLEX2: a complete structure solution, refinement and analysis program, *Journal of Applied Crystallography*, (2009), 2, 42, 339-41
- (40)L. Farrugia, WinGX and ORTEP for Windows: an update, *Journal of Applied Crystallography*, (2012), 4, 45, 849-54

For Table of Contents Only



R=H, Me, MeO, tert-butyl, Cl, NO₂